Identification and characterization of a novel folliculin-interacting protein FNIP2

Hisashi Hasumi[1,#], **Masaya Baba**[1,#], **Seung-Beom Hong**[1], **Yukiko Hasumi**[1], **Ying Huang**[3], **Masahiro Yao**[3], **Vladimir A. Valera**[1], **W. Marston Linehan**[1], and **Laura S. Schmidt**[1,2]

[1]Urologic Oncology Branch, Center for Cancer Research, National Cancer Institute, National Institutes of Health, Bethesda, Maryland, 20894

[2]Basic Research Program, SAIC-Frederick, Inc., National Cancer Institute-Frederick, Frederick, Maryland 21702

[3]Department of Urology and Molecular Genetics, Yokohama City University Graduate School of Medicine, Yokohama, Japan

Abstract

Birt-Hogg-Dube' syndrome characterized by increased risk for renal neoplasia is caused by germline mutations in the *BHD/FLCN* gene encoding a novel tumor suppressor protein, folliculin(FLCN), which interacts with FNIP1 and 5′-AMP-activated protein kinase(AMPK). Here we report the identification and characterization of a novel FNIP1 homolog FNIP2 that also interacts with FLCN and AMPK. C-terminally-deleted FLCN mutants, similar to those produced by naturally-occurring germline mutations in BHD patients, were unable to bind FNIP2. These data taken together with our previous results that demonstrated FNIP1 binding to the C-terminus of FLCN suggest that FLCN tumor suppressor function may be facilitated by interactions with both FNIP1 and FNIP2 through its C-terminus. Furthermore, we demonstrate that FNIP1 and FNIP2 are able to form homo- or heteromeric multimers suggesting that they may function independently or cooperatively with FLCN. Differential expression of *FNIP1* and *FNIP2* transcripts in some normal tissues may indicate tissue specificity for these homologs. Interestingly *FNIP1* and *FNIP2* were oppositely expressed in human clear cell renal cell carcinoma(RCC), and coordinately expressed in chromophobe RCC and oncocytoma, suggesting their differential function in different histologic variants of RCC.

Keywords

1. Introduction

Birt-Hogg-Dubé (BHD) syndrome is an inherited genodermatosis with an increased risk of renal neoplasia (Birt et al., 1977; Toro et al, 1999; Zbar et al., 2002) caused by germline mutations in the *BHD(FLCN)* gene located at chromosome 17p11.2 (Nickerson et al., 2002). Nearly all BHD mutations identified to date, which include frameshift, splice-site or nonsense mutations, are predicted to prematurely truncate the BHD protein, folliculin (FLCN) (Nickerson et al., 2002; Khoo et al., 2002; Schmidt et al., 2005; Leter et al., 2007). Renal tumors, which develop most frequently in BHD patients, include chromophobe renal cell

Address for correspondence: Dr. Laura S. Schmidt, National Cancer Institute-Frederick, Bldg 560, Rm 12-69, Frederick, MD 21702; phone: 301-846-5856; fax: 301-846-6145; email: schmidtl@ncifcrf.gov.
[#]These authors contributed equally to this work.

carcinoma(RCC) and renal oncocytic hybrid tumors (Pavlovich et al., 2002; Pavlovich et al., 2005; Murakami et al., 2007). *BHD* may function as a tumor suppressor gene since somatic mutations in the remaining wild-type copy of *BHD* or loss of heterozygosity at chromosome 17p11.2 have been identified in BHD-associated renal tumors (Vocke et al., 2005). Moreover in the Nihon rat model of *BHD* inactivation, restoration of *BHD* expression in the rat suppresses renal tumorigenesis (Togashi et al., 2006).

Folliculin is a novel 64-kDa protein without characteristic domains to suggest function (Nickerson et al., 2002). We recently identified FNIP1, a novel folliculin-interacting protein, which also binds to 5′-AMP-activated protein kinase (AMPK) (Baba et al., 2006), an important energy sensor in cells that negatively regulates the master switch for cell growth and proliferation, mammalian target of rapamycin (mTOR) (Inoki et al., 2005). FLCN and FNIP1 phosphorylation levels were affected by AMPK and mTOR activities suggesting a functional relationship with the AMPK-mTOR pathway. Mutations in several other tumor suppressor genes have been shown to result in dysregulation of mTOR signaling leading to the development of other hamartoma syndromes. Here we report the identification of another novel FLCN binding protein FNIP2 (KIAA1450, GenBank accession no. **NM 020840**) with homology to FNIP1 (49% identity, 74% similarity), which is conserved across species, and also binds to AMPK. Interestingly, FNIP1 and FNIP2 were able to form homo- and heteromeric multimers suggesting a coordinated functional relationship between these proteins. We evaluated expression patterns of *FLCN, FNIP1* and *FNIP2* in normal human tissues, and compared their expression in sporadic RCC and normal kidney.

2. Materials and methods

2.1. FNIP2 identification and bioinformatic analysis

KIAA1450 (GenBank accession no. **NM 020840**) was identified as a FNIP1 homolog by bioinformatic searching of available sequence databases using BLAST (Altschul et al., 1990). ClustalX (1.8) interface with pairwise gap openings and gap extension penalties set at 10x and 0.2x, respectively, was used for the ClustalW multiple sequence alignment program to prepare multiple alignments of FNIP1, FNIP2 and their homologs. The distances between all pairs of sequences (percent divergence) were calculated from the multiple alignments using ClustalX and the neighbor-joining method (Saitou and Nei, 1987) was applied to the distance matrix. The unrooted phylogenetic tree was represented with the help of the Treeview 1.6.6 software (Page, 1996).

2.2. Cell lines and cell culture

HEK293 cells expressing doxycycline-inducible HA-FNIP2 were established using the Flp-In T-Rex System (Invitrogen, Carlsbad, CA) according to the manufacturer's protocol. HEK293 cells were cultured in Dulbecco's modified Eagle medium (DMEM; Invitrogen) supplemented with 10% tet-screened fetal bovine serum (Hyclone, Logan, UT) and antibiotics (penicillin/ streptomycin).

2.3. Antibodies

Normal rabbit immunoglobulin (IgG; Santa Cruz Biotechnology, Santa Cruz, CA), HRP-labeled anti-mouse and anti-rabbit secondary antibodies (Vector Laboratories, Burlingame, CA), AMPKα mouse monoclonal(F6), AMPKα, and AMPKβ1 rabbit polyclonal antibodies (Cell Signaling, Beverly, MA), AMPKγ1 rabbit polyclonal antibody (Zymed, San Francisco, CA), HA and Flag rabbit polyclonal antibodies (Santa Cruz Biotechnology), V5 rabbit polyclonal antibody (Sigma Aldrich, St. Louis, MO), and HA rat monoclonal(3F10) antibody (Roche Applied Science, Indianapolis, IN) were used according to manufacturer's protocol. FNIP1-189 rabbit polyclonal antibody was generated against a His6X- tagged recombinant

protein corresponding to codons 765-929 of FNIP1. FNIP2-3G and FNIP2-4G rabbit polyclonal antibodies were raised against FNIP2 peptide CSRDLGLKPDKEANR and FNIP2 peptide CDKGFAEDRGSRND, respectively. We chose non-homologous regions to use as antigens to generate FNIP1 and FNIP2 antibodies, and these antibodies were confirmed not to cross react with each other. FLCN-105 rabbit polyclonal antibody was raised against GST-FLCN and FLCN monoclonal antibody (FLCN-mAb) was raised against full length GST-FLCN in the mouse. Culture medium from a single clone hybridoma cell line was used as the antibody source.

2.4. Immunoprecipitation and western blotting

Cells were lysed in lysis buffer [20mM Tris-HCl, 150mM NaCl, 5% glycerol, 0.1% TritonX-100, Complete Protease Inhibitor Cocktail, Phostop Phosphatase Inhibitor Cocktail (Roche Applied Science)] and immunoprecipitated at 4°C overnight with protein G-Sepharose (GE Healthcare Bioscience, Piscataway, NJ) bound antibodies, anti-HA affinity matrix (Roche Applied Science), anti-V5-Agarose or anti-Flag M2-Agarose(Sigma Aldrich). For sequential immunoprecipitation, cell lysates were immunoprecipitated with anti-HA affinity matrix overnight. Immunoprecipitates were washed five times followed by elution with HA-peptide (Roche Applied Science) competition as described previously (Baba et al., 2006). Eluted protein was diluted with lysis buffer and immunoprecipitated with anti-Flag M2-Agarose overnight. The resin was washed five times with lysis buffer and proteins were eluted with sodium dodecyl (SDS)-containing sample buffer followed by boiling and subjected to SDS-polyacrylamide gel (SDS-PAGE) electrophoresis. ReliaBlot (Bethyl Laboratories, Montgomery, TX) was used for rabbit polyclonal western blotting to detect proteins immunoprecipitated by rabbit polyclonal antibodies.

2.5. Immunofluorescence microscopy

Immunofluorescence microscopy of MCF7 cells transfected with FNIP2-Flag and HA-FLCN was performed as previously described (Baba et al., 2006). Alexa488 conjugated goat anti-rabbit antibody and Alexa594 conjugated goat anti-rat antibody (Invitrogen) were used as secondary antibodies. Images were obtained by confocal microscopy.

2.6. Plasmids, transfection, recombinant protein expression and purification

The Gateway® Protein Expression System (Invitrogen) was used to produce a variety of expression vectors encoding full-length FLCN, FNIP1 and FNIP2. GST-fusion FLCN deletion mutants were produced in bacmid-infected Sf9 cells as previously described (Baba et al., 2006). Transfections were performed using Lipofectamine 2000 (Invitrogen) according to the manufacturer's protocol.

2.7. In vitro binding assay

GST-fusion proteins were immobilized on glutathione-Sepharose beads (GE Healthcare) and incubated with ^{35}S-labeled *in vitro* translated FNIP2 prepared using TNT T7 Quick kit (Promega, Madison, WI). After washing, beads were boiled with SDS-containing sample buffer and subjected to SDS-PAGE, followed by Coomassie Brilliant Blue (CBB) staining and autoradiography.

2.8. Quantitative Real Time-PCR(qRT-PCR)

qRT-PCR of human normal tissue was performed using TissueScan Real-Time Human-48 tissues (Origene, Rockville, MD), Power SYBR Green PCR Master Mix and 7300 Real Time PCR System (Applied Biosystems, Foster City, CA) according to the manufacturer's protocol. Sequence specific primers were designed using Primer Express computer software (Applied Biosystems). The primer sequences were: *FLCN* forward, 5′-TGC AGG TGC TGG TGA AGG

TAA CCT-3′and *FLCN* reverse, 5′-GGG ATT GGG CAA GTC AGA TGC TTG-3′; *FNIP1* forward, 5′-TTT GTT CCT CCC CAC TGC TTC CCA-3′and *FNIP1* reverse, 5′-AGT AGC AGC AGC TCA TTC CTT GGG-3′; *FNIP2* forward, 5′-CAC CCC ACA TCC GTT TCT CAT TAC G-3′ and *FNIP2* reverse, 5′-CCC TGG AAG GTG GTG AAT GAG GGA A-3′. All quantities were normalized to β actin measured with β actin primer provided by the manufacturer.

To investigate the expression levels of *FLCN*, *FNIP1* and *FNIP2* in renal tumors, qRT-PCR analysis was carried out with 106 sporadic renal tumor specimens and 37 normal kidney specimens obtained under an institutional review board-approved clinical protocol with patient informed consent. The isolation of total RNA, cDNA preparation and qRT-PCR with Taq-Man fluorescent probes for the measurement of gene expression were performed essentially as previously described (Yao et al., 2005; Yao et al., 2007). Primer sequences are: *FNIP1* forward, 5′-AGA TTG GGC AGA AGA GGA TGA G-3′, *FNIP1* reverse, 5′-TTG GCA ATG TTG GGC TGA-3′, *FNIP1* TaqMan probe, 5′-CCT GGG TCA AGG TTA ATC GAA GTG AGT GCT G-3′; *FNIP2* forward, 5′-GGT CCT TGG AAG TGG AGC TG-3′, *FNIP2* reverse, 5′-GTG AGC GGC AAA GT TCC T-3′, *FNIP2* TaqMan probe 5′-CAA GGT CTC AGA GCA TCA GCA CCC AGA-3′.

2.9. Statistical analysis

The Mann—Whitney U-test was used to test for differences in distribution between groups. All statistical analysis was performed with SPSS software (version 10.1, SPSS, Inc., Chicago, IL). All statistical tests were two-sided and were considered to be statistically significant for $p < 0.05$.

3. Results and Discussion

3.1. Identification of FNIP2 and evolutionary divergence among FNIP1 and FNIP2 homologs

We have identified a human uncharacterized cDNA, KIAA1450, that encodes a human FNIP1 homolog by bioinformatic searching of available sequence databases using BLAST (Altschul et al., 1990) and designated it FNIP2 (folliculin interacting protein 2). The KIAA1450 transcript (GenBank accession no. **NM 020840**) had a 177bp sequence with a remarkably high GC content upstream of the ATG initiation codon, and we found an in-frame TGA termination codon, which resided in the 5′ end of the GC rich region. This finding enabled us to confirm the ATG initiation codon. Human FNIP1 and FNIP2 display high homology in the N-terminal half of the proteins and in a 158 residue block within the C-terminus, but low similarity in the other regions, suggesting that the regions of high homology may be important for critical functions (e.g., FLCN interaction), and the regions of low homology may contribute to the unique characteristics of each homolog. Overall, FNIP1 and FNIP2 proteins show 49% identity and 74% similarity, respectively (Fig.1A). Vertebrates from human to *Xenopus* have both *FNIP1* and *FNIP2* transcripts [human *FNIP1*(GenBank accession no. **DQ145719**), mouse *FNIP1* (GenBank accession no. **NM 173753**), X.tropicalis *FNIP1*(Ensembl **ENSXETP00000036209**), human *FNIP2* (GenBank accession no. **NM 020840**), mouse *FNIP2* (GenBank accession no. **XM 907047**), *X. tropicalis FNIP2* (Ensembl **ENSXETG00000016579**)]. *D. melanogaster* (GenBank accession no. **NM 140686**) and *C.elegans* (Wormbase **T04C4.1**) each have a single transcript encoding a protein that shows homology to both FNIP1 and FNIP2. Seven amino acid sequence blocks in FNIP2 that were conserved across all species from human to *C. elegans* with similarity >30% were identified. Although there are no known functional domains in FNIP2, the conserved sequence blocks may represent regions important to FNIP2 function (Fig.1 B).

To gain insight into the evolutionary relationships among FNIP1, FNIP2 and their homologs, we compared the amino acid sequences of these proteins and constructed a phylogenetic tree (Fig.1C; sequence alignment available as Supplemental Figure 1). Human FNIP1 and its homologs formed a cluster distinct from human FNIP2 and its homologs. Within each FNIP cluster, the mammalian proteins clustered separately from the *Xenopus* proteins. As expected, the *Drosophila* and *Caenorhabditis* species, each of which has a single FNIP protein, displayed the greatest divergence from the FNIP1 and FNIP2 branching clusters.

3.2. Analysis of expression patterns of FLCN, FNIP1 and FNIP2 in normal human tissues

To analyze gene expression patterns of *FLCN*, *FNIP1* and *FNIP2* in human tissues, quantitative Real Time PCR (qRT-PCR) was performed (Fig.2A). Expression patterns of *FLCN, FNIP1* and *FNIP2* were generally similar, and coordinately high in certain tissues including muscle, nasal mucosa, salivary gland and uvula, suggesting that FLCN, FNIP1 and FNIP2 may cooperate together in those organs. *FLCN* expression was rather ubiquitous compared to *FNIP1* and *FNIP2*. Interestingly *FNIP2* expression was higher relative to *FNIP1* in fat, liver and pancreas, which may suggest that FNIP2 has a specific function in those metabolic tissues.

3.3. Interaction of FNIP2 with FLCN and AMPK and subcellular localization

Based on the structural similarity between FNIP1 and FNIP2, FNIP2 binding to FLCN and AMPK was evaluated. HEK293 cells expressing HA-FNIP2 in a doxycycline-dependent manner were lysed and immunoprecipitated with anti-HA antibody followed by western blotting to identify co-immunoprecipitated endogenous FLCN and AMPK subunits. Endogenous FLCN and all of the AMPK subunits (α,β and γ) were co-immunoprecipitated with HA-FNIP2 (Fig.3A). Endogenous FLCN and AMPK were also co-immunoprecipitated with endogenous FNIP2 in an anti-FNIP2 immunoprecipitation (Fig.3B). Furthermore co-transfected HA-FLCN and FNIP2-Flag colocalized in the cytoplasm in a reticular pattern, which was identical to the FLCN/FNIP1 colocalization pattern (Baba et al., 2006). FLCN localized both in the cytoplasm and nucleus in a reticular pattern whereas FNIP2 localized only in the cytoplasm (Fig3C). In order to show a direct interaction between FLCN and FNIP2 and to determine the FNIP2 binding domain in FLCN, we performed an *in vitro* binding assay with full length GST-FLCN or GST-FLCN deletion mutants, and *in vitro* translated ^{35}S- labeled FNIP2. Full-length GST-FLCN and N-terminal GST-FLCN deletion mutants that retained the C-terminus were able to bind to FNIP2. However, C-terminally deleted GST-FLCN mutants could not bind to FNIP2 (Fig.3D). Interestingly the majority of *BHD* mutations found in BHD patients result in an altered reading frame predicted to prematurely truncate FLCN thereby abrogating its ability to bind FNIP2. The finding that FLCN binding to FNIP2 is lost as a consequence of *BHD* mutations resulting in the BHD phenotype suggests that the interaction between FLCN and FNIP2 is functionally important.

3.4. Identification of multimeric molecular complexes containing FNIP1 and FNIP2

Our results demonstrate that FNIP1 and FNIP2 share many characteristics. FNIP1 and FNIP2 are structurally similar, display identical interactions with FLCN and AMPK, and show similar subcellular localization patterns. However, there are also distinct differences between FNIP1 and FNIP2. With the exception of the last 158 amino acids, the homology between FNIP1 and FNIP2 in the C-terminal half of the proteins is low. These non-homologous regions of FNIP1 and FNIP2 may characterize their specific functions (Fig.1A). *FNIP1* and *FNIP2* mRNA expression levels in human tissues were similar but in some tissues these two mRNAs were expressed in an opposing fashion or at dramatically different levels (i.e., higher FNIP2 expression in pancreas and higher FNIP1 expression in parathyroid gland [Fig.2A]). These data may suggest that FNIP1 and FNIP2 each play a specific role in certain tissues or that the ratio of FNIP1 to FNIP2 has physiologic significance. To analyze the relationship between

FNIP1, FNIP2 and FLCN, we tested the ability of FNIP1 and FNIP2 to interact in the presence and absence of FLCN overexpression. V5-FNIP1 and Flag-FNIP2 were co-transfected into HEK293 cells, which expressed HA-FLCN in a doxycycline-dependent manner. In both doxycycline-induced HA-FLCN-expressing cells and in uninduced cells, V5-FNIP1 and Flag-FNIP2 co-immunoprecipitated in a reciprocal fashion (Fig.4A). These data indicate that FNIP1 and FNIP2 were able to form hetero-multimers in a FLCN-independent manner. Endogenous FNIP1 and FNIP2 also co-immunoprecipitated from HEK 293 cells supporting the existence of a naturally-occurring FNIP1/FNIP2 hetero-multimer (Fig.4B). We performed an *in vitro* binding assay with GST-FNIP1 or GST-FNIP1 deletion mutants, and ^{35}S-labeled *in vitro* translated FNIP2 to identify the FNIP2 binding region in FNIP1 and to confirm their direct interaction with each other. Full length GST-FNIP1 interacted with FNIP2, and all GST-FNIP1 deletion mutants that contained 2 of the 5 sequence blocks, which were conserved across species (Baba et al., 2006), were able to interact with FNIP2 (Fig. 4C). These findings suggest that these FNIP1 conserved sequences are important for recognition and binding to FNIP2.

In order to characterize the FNIP1/FNIP2/FLCN/AMPK complex, we purified the FNIP1 homo-multimer, FNIP2 homo-multimer and FNIP1/FNIP2 hetero-multimer by sequential immunoprecipitation from HEK 293 cells expressing FNIP1 and FNIP2 with different epitope tags. The HA-immunoprecipitates were eluted by HA-peptide competition followed by immunoprecipitation with anti-Flag, which enabled us to purify protein complexes that had both HA- and Flag-tagged proteins. Immunoprecipitates were detected by antibodies against FLCN, AMPKγ, HA and Flag epitope tags, indicating that all of the possible multimers-FNIP1 homo-multimer, FNIP2 homo-multimer and FNIP1/FNIP2 hetero-multimer-had the ability to interact with FLCN and AMPK (Fig.4D). Further analysis to characterize the nature of each multimer will clarify the functional significance of these multimeric complexes.

3.5. FNIP1 and FNIP2 mRNA expression levels in sporadic renal cell carcinoma (RCC) and normal kidney tissue

BHD germline mutations predispose patients to develop kidney tumors, predominantly oncocytic hybrid tumors, chromophobe RCC and oncocytoma. Since FNIP1 and FNIP2 interact with FLCN, which is encoded by the *BHD* gene, these proteins may play a role in renal carcinogenesis. To investigate the relationship between *FLCN*, *FNIP1* and *FNIP2* expression and sporadic RCC, we performed quantitative RT-PCR with mRNA isolated from 106 cases of sporadic renal tumors and 37 cases of normal kidney tissue. There were no significant differences in *FLCN* mRNA expression levels between normal kidney tissue and sporadic renal tumor tissue (Fig. 5A). Interestingly, *FNIP1* mRNA was significantly higher in clear cell RCC compared to normal kidney (clear cell RCC vs normal kidney: median=2.197 vs 1.624, $p<0.001$;Fig. 5B). Conversely *FNIP2* mRNA was significantly lower in clear cell RCC compared to normal kidney (clear cell RCC vs normal kidney: median=0.197 vs 1.517, $p<0.001$; Fig. 5C). Furthermore, *FNIP1* mRNA was significantly higher in chromophobe RCC (chromophobe RCC vs normal kidney: median=2.965 vs 1.624, $p=0.003$) and *FNIP2* mRNA was significantly higher in oncocytoma compared to normal kidney (oncocytoma vs normal kidney: median=2.261 vs 1.517, $p=0.019$). The physiological significance of elevated *FNIP1* and *FNIP2* expression in sporadic chromophobe RCC and oncocytoma is unclear. However it is remarkable that *FNIP1* and *FNIP2* expression levels were higher in histologic types of renal tumors that are frequently seen in BHD patients, suggesting the existence of a common pathway for the development of sporadic chromophobe RCC/oncocytoma and BHD-related kidney tumors. It is also interesting that *FNIP1* expression levels in sporadic clear cell RCC were higher than in normal kidney, whereas *FNIP2* expression levels in sporadic clear cell RCC were lower than in normal kidney. Although the physiological significance of higher *FNIP1* and lower *FNIP2* mRNA expression levels in sporadic clear cell RCC is unknown, these data may suggest a possible involvement of FLCN/FNIP1/FNIP2 signaling pathways in

sporadic clear cell carcinogenesis. The opposing expression levels of *FNIP1* and *FNIP2* specific to sporadic clear cell RCC may suggest unique molecular functions for these homologous proteins. Alternatively the relative ratio of *FNIP1* to *FNIP2* may affect the formation of homo- or hetero-multimers, and consequently, their physiologic role in normal and neoplastic kidney cells. It will be very important to elucidate the physiologic function of FNIP1 and FNIP2 as well as FLCN in normal cells in order to understand the role of these proteins in BHD syndrome and sporadic renal carcinogenesis.

4. Conclusions

In summary, we have identified a novel FLCN-interacting protein, FNIP2, with homology to FNIP1 that is conserved across species. FNIP2 interacts with the C-terminal half of the folliculin tumor suppressor protein and with an important nutrient- and energy-sensing molecule, AMPK, a negative regulator of mTOR. Importantly we demonstrate that FNIP1 and FNIP2 can form multimers independent of FLCN expression, suggesting that they may function independently or cooperatively with FLCN. Their differential expression in human tissues may indicate tissue-specific roles for *FNIP1* and *FNIP2* in normal cell signaling. Moreover, the elevated expression levels of *FNIP1* and *FNIP2* in the histologic variants of renal tumors found most often in BHD patients may suggest a common pathway for the development of BHD-associated renal tumors, sporadic chromophobe RCC and sporadic oncocytoma.

Acknowledgements

Abbreviations

BHD, Birt-Hogg-Dube'syndrome; FLCN, folliculin; FNIP1, folliculin interacting protein1; FNIP2, folliculin interacting protein 2; AMPK, 5′AMP-activated protein kinase; mTOR, mammalian target of rapamycin; RCC, renal cell carcinoma; GST, glutathione-S-transferase; HEK, human embryonic kidney; qRT, quantitative real time.

References

Altschul SF, Gish W, Miller W, Myers EW, Lipman DJ. Basic local alignment search tool. J. Mol. Biol 1990;215:403–410. [PubMed: 2231712]

Baba M, et al. Folliculin encoded by the BHD gene interacts with a binding protein, FNIP1, and AMPK, and is involved in AMPK and mTOR signaling. Proc. Natl. Acad. Sci. USA 2006;103:15552–15557. [PubMed: 17028174]

Birt AR, Hogg GR, Dube WJ. Hereditary multiple fibrofolliculomas with trichodiscomas and acrochordons. Arch. Dermatol 1977;113:1674–1677. [PubMed: 596896]

Inoki K, Corradetti MN, Guan KL. Dysregulation of the TSC-mTOR pathway in human disease. Nat. Genet 2005;37:19–24. [PubMed: 15624019]

Khoo SK, et al. Clinical and genetic studies of Birt-Hogg-Dube syndrome. J. Med. Genet 2002;39:906–912. [PubMed: 12471204]

Leter EM, Koopmans AK, Gille JJ, van Os TA, Vittoz GG, David EF, Jaspars EH, Postmus PE, van Moorselaar RJ, Craanen ME, Starink TM, Menko FH. Birt-Hogg-Dube Syndrome: Clinical and Genetic Studies of 20 Families. J. Invest. Dermatol 2008;128:45–49. [PubMed: 17611575]

Murakami T, Sano F, Huang Y, Komiya A, Baba M, Osada Y, Nagashima Y, Kondo K, Nakaigawa N, Miura T, Kubota Y, Yao M, Kishida T. Identification and characterization of Birt-Hogg-Dube associated renal carcinoma. J. Pathol 2007;211:524–531. [PubMed: 17323425]

Nickerson ML, et al. Mutations in a novel gene lead to kidney tumors, lung wall defects, and benign tumors of the hair follicle in patients with the Birt-Hogg-Dube syndrome. Cancer Cell 2002;2:157–164. [PubMed: 12204536]

Page RDM. TREEVIEW: An application to display phylogenetic trees on personal computers. Computer Applications in the Biosciences 1996;12:357–358. [PubMed: 8902363]

Pavlovich CP, Walther MM, Eyler RA, Hewitt SM, Zbar B, Linehan WM, Merino MJ. Renal tumors in the Birt-Hogg-Dube syndrome. Am. J. Surg. Pathol 2002;26:1542–1552. [PubMed: 12459621]

Pavlovich CP, Grubb RL 3rd, Hurley K, Glenn GM, Toro J, Schmidt LS, Torres-Cabala C, Merino MJ, Zbar B, Choyke P, Walther MM, Linehan WM. Evaluation and management of renal tumors in the Birt-Hogg-Dube syndrome. J. Urol 2005;173:1482–1486. [PubMed: 15821464]

Saitou N, Nei M. The neighbor-joining method: a new method for reconstructing phylogenetic trees. Mol Biol Evol 1987;4:406–425. [PubMed: 3447015]

Schmidt LS, et al. Germline BHD-mutation spectrum and phenotype analysis of a large cohort of families with Birt-Hogg-Dube syndrome. Am. J. Hum. Genet 2005;76:1023–1033. [PubMed: 15852235]

Togashi Y, Kobayashi T, Momose S, Ueda M, Okimoto K, Hino O. Transgenic rescue from embryonic lethality and renal carcinogenesis in the Nihon rat model by introduction of a wild-type Bhd gene. Oncogene 2006;25:2885–2889. [PubMed: 16369488]

Toro JR, Glenn GM, Duray PH, Darling T, Weirich G, Zbar B, Linehan WM, Turner ML. Birt-Hogg-Dube Syndrome: A Novel Marker of Kidney Neoplasia. Arch. Dermatol 1999;135:1195–1202. [PubMed: 10522666]

Vocke CD, Yang Y, Pavlovich CP, Schmidt LS, Nickerson ML, Torres-Cabala CA, Merino MJ, Walther MM, Zbar B, Linehan WM. High Frequency of Somatic Frameshift BHD Gene Mutations in Birt-Hogg-Dube-Associated Renal Tumors. J. Natl. Cancer Inst 2005;97:931–935. [PubMed: 15956655]

Yao M, Tabuchi H, Nagashima Y, Baba M, Nakaigawa N, Ishiguro H, Hamada K, Inayama Y, Kishida T, Hattori K, Yamada-Okabe H, Kubota Y. Gene expression analysis of renal carcinoma: adipose differentiation-related protein as a potential diagnostic and prognostic biomarker for clear-cell renal carcinoma. J. Pathol 2005;205:377–387. [PubMed: 15682440]

Yao M, Huang Y, Shioi K, Hattori K, Murakami T, Nakaigawa N, Kishida T, Nagashima Y, Kubota Y. Expression of adipose differentiation-related protein: a predictor of cancer-specific survival in clear cell renal carcinoma. Clin. Cancer Res 2007;13:152–160. [PubMed: 17200350]

Zbar B, et al. Risk of renal and colonic neoplasms and spontaneous pneumothorax in the Birt-Hogg-Dube syndrome. Cancer Epidemiol. Biomarkers Prev 2002;11:393–400. [PubMed: 11927500]

Figure 1.
Identification of *FNIP2* and evolutionary divergence among FNIP1 and FNIP2 homologs. (A) Amino acid sequence alignment of human FNIP1 and FNIP2 with 49% identity and 74% similarity. Asterisk, identity; dots, similarity. (B) Evolutionarily conserved sequence blocks in FNIP2. The sequences were aligned with ClustalX (1.8). Seven conserved sequence blocks were identified with similarities > 30%. (C) The phylogenetic tree for the FNIP1 and FNIP2 proteins. The tree was constructed from a multiple alignment of FNIP1 and FNIP2 protein sequences from human, mouse, *Xenopus*, *Drosophila* and *Caenorhabditis* by the neighbor-joining method. A distance scale bar is indicated.

Figure 2.
Relative mRNA expression levels of *FLCN, FNIP1* and *FNIP2* in human tissues analyzed by qRT-PCR. (A) *FLCN* (black), *FNIP1* (red) and *FNIP2* (blue) expression levels. Mean+standard deviation (SD). (B) FNIP2 immunohistochemistry staining in tubules of normal human kidney.
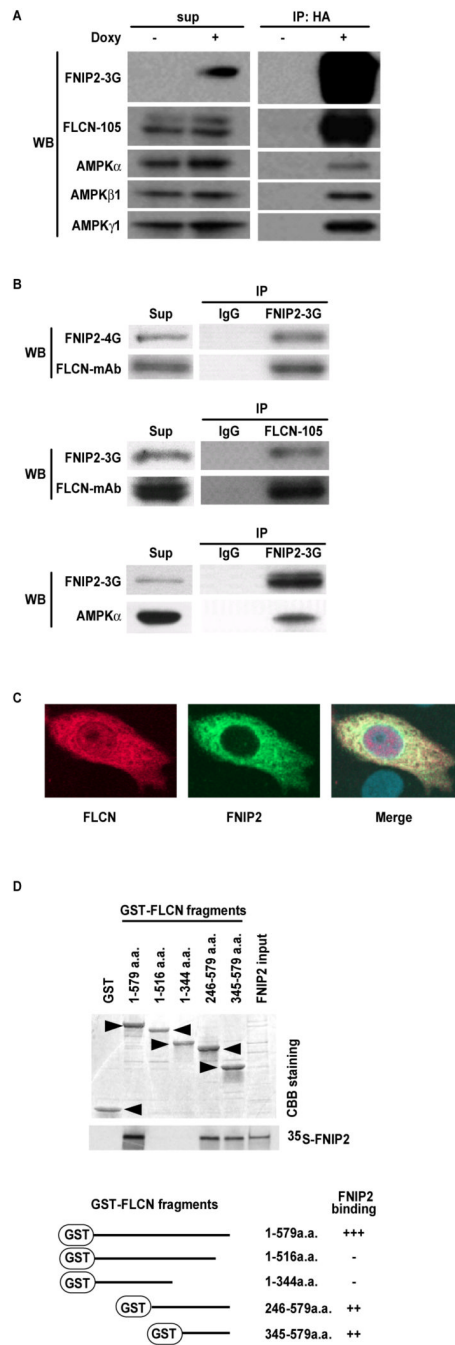
Figure 3.
FNIP2 interaction with FLCN and AMPK and its subcellular localization. (A) Co-immunoprecipitation of endogenous FLCN and AMPK subunits with HA-FNIP2. Doxycycline-inducible HA-FNIP2 expressing HEK 293 cell lysates were immunoprecipitated with anti-HA antibody and blotted with antibodies as indicated, showing that FLCN and AMPK subunits interact with FNIP2. (B) Endogenous interaction of FNIP2 with FLCN and AMPK. HEK293 cell lysates were immunoprecipitated with control IgG, anti-FNIP2 (FNIP2-3G) and anti-FLCN (FLCN-105) antibodies followed by western blotting with indicated antibodies. (C) Cytoplasmic co-localization of FLCN and FNIP2 with a reticular pattern. HA-FLCN and FNIP2-Flag co-transfected into MCF7 cells were detected with anti-HA and anti-FNIP2

(FNIP2-3G) antibodies. Red, HA-FLCN; Green, FNIP2-Flag; Blue, DAPI. (D) C-terminus of FLCN is critical for FNIP2 binding. Recombinant GST-FLCN and GST-FLCN deletion mutants expressed in Sf9 cells were immobilized on glutathione-Sepharose beads and incubated with ^{35}S-labeled *in vitro* translated (IVT) FNIP2. FNIP2 binding was evaluated by SDS-PAGE followed by autoradiography. CBB (Coomaissee Brillant Blue) staining shows relative expression of the GST-FLCN fragments.
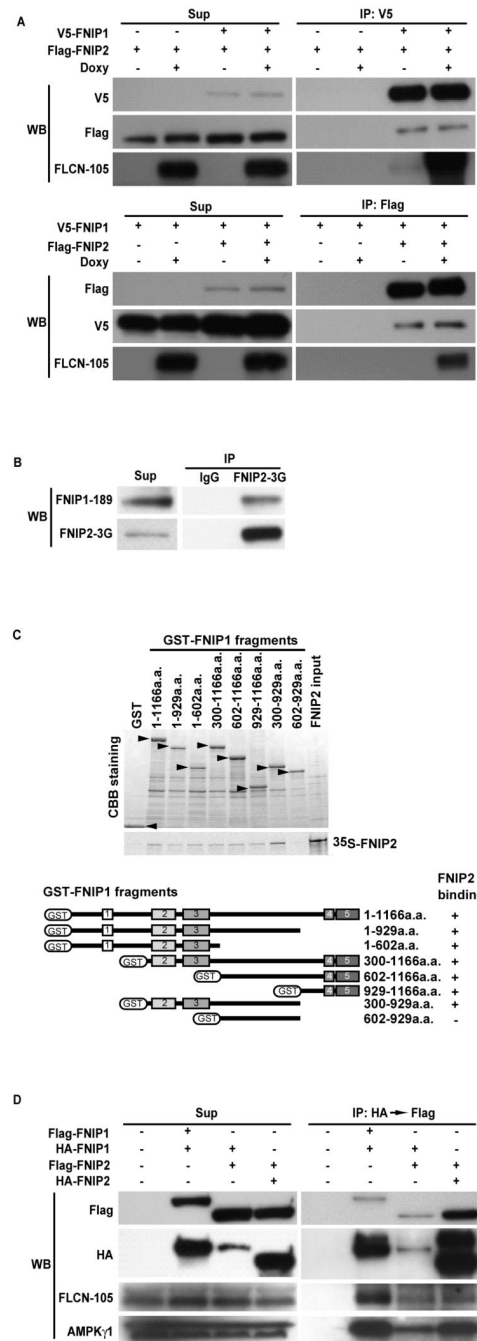
Figure 4.
FNIP1 and FNIP2 multimer formation. (A) Doxycycline-inducible HA-FLCN-expressing HEK293 cells co-transfected with V5-FNIP1 and Flag-FNIP2 were immunoprecipitated with anti-V5 or anti-Flag antibody followed by western blotting with indicated antibodies. V5-FNIP1 and Flag-FNIP2 were reciprocally co-immunoprecipitated independent of FLCN overexpression. (B) Endogenous FNIP1 and FNIP2 form a multimer. Control IgG or anti-FNIP2(FNIP2-3G) immunoprecipitates from HEK293 cells were separated by SDS-PAGE followed by western blotting with anti-FNIP1(FNIP1-189) and anti-FNIP2(FNIP2-3G) antibodies. (C) FNIP1 conserved domains contribute to FNIP2 binding. Recombinant GST-FNIP1 and GST-FNIP1 deletion mutants expressed in Sf9 cells were immobilized on

glutathione-Sepharose beads and incubated with ^{35}S-*in vitro* translated (IVT) FNIP2. FNIP2 binding was evaluated by SDS-PAGE followed by autoradiography. CBB staining shows relative expression of the GST-FNIP1 fragments. The numbered blocks in the diagram indicate FNIP1 sequence blocks conserved across species (Baba et al., 2006). (D) All homo- and hetero-multimers of FNIP1 and FNIP2 are able to bind FLCN and AMPK. To purify all possible FNIP1/FNIP2 molecular complexes, HA-FNIP1, Flag-FNIP1, Flag-FNIP2 and HA-FNIP2 expression vectors were transfected into HEK293 cells in combinations as indicated. HA-immunoprecipitates of cell lysates were eluted by HA peptide competition followed by sequential immunopurification by anti-Flag antibody. Final immunoprecipitates were boiled with SDS-sample buffer followed by western blotting with antibodies indicated.

A FLCN

	clear	papillary	chromo	onco	collecting	normal
n=	52	21	16	10	7	37
median=	3.098	2.791	2.586	2.757	3.914	2.728

Mann-Whitney U-test

	papillary	chromo	onco	collecting	normal
clear	0.495	0.942	0.848	0.761	0.332
papillary		0.602	0.704	0.326	0.994
chromo			0.752	0.504	0.574
onco				0.626	0.677
collecting					0.282

B FNIP1

	clear	papillary	chromo	onco	collecting	normal
n=	52	21	16	10	7	37
median=	2.197	1.638	2.965	1.463	2.555	1.624

Mann-Whitney U-test

	papillary	chromo	onco	collecting	normal
clear	0.015	0.148	0.301	0.623	<0.001
papillary		0.014	0.933	0.145	0.910
chromo			0.126	0.385	0.003
onco				0.495	0.677
collecting					0.052

C FNIP2

	clear	papillary	chromo	onco	collecting	normal
n=	52	21	16	10	7	37
median=	0.197	1.134	2.201	2.261	1.201	1.517

Mann-Whitney U-test

	papillary	chromo	onco	collecting	normal
clear	<0.001	<0.001	<0.001	0.001	<0.001
papillary		0.046	0.030	0.542	0.234
chromo			0.551	0.535	0.096
onco				0.417	0.019
collecting					0.860

Figure 5.
FLCN, *FNIP1* and *FNIP2* mRNA expression analysis in sporadic renal cell carcinoma and normal kidney. *FLCN*(A), *FNIP1*(B) and *FNIP2*(C) mRNA levels in human clinical samples were evaluated by qRT-PCR. The gene expression levels are shown by dot and box-whisker plots. *FLCN* mRNA expression in normal kidney and tumors of various histologies was not significantly different. *FNIP1* expression was significantly higher in clear cell and chromophobe RCC relative to normal kidney. Marginally higher *FNIP1* mRNA levels were detected in collecting duct carcinoma compared to normal kidney. *FNIP2* mRNA levels were significantly lower in clear cell RCC and higher in oncocytoma relative to normal kidney. Box,

borders of the 25% and 75% quartiles; horizontal bar, median value; whiskers, ranges in each group; vertical axis, relative gene expression by qRT-PCR; horizontal axis, tumor categories.